Journal of Applied Physics ARTICLE scitation.org/journal/jap

A novel vibrational spectroscopy using spintronic–plasmonic antennas: Magneto-refractive surface-enhanced infrared absorption

Cite as: J. Appl. Phys. **129**, 073103 (2021); doi: 10.1063/5.0036385
Submitted: 4 November 2020 · Accepted: 1 February 2021 ·
Published Online: 18 February 2021

Gaspar Armelles,[1,a)] Luca Bergamini,[2,3] Alfonso Cebollada,[1] Nerea Zabala,[2,3] and Javier Aizpurua[3]

AFFILIATIONS

[1]Instituto de Micro y Nanotecnología, IMN-CNM-CSIC, Isaac Newton, 8, Tres Cantos, Madrid 28760, Spain
[2]Department of Electricity and Electronics, FCT-ZTF, UPV-EHU, Bilbao 48080, Spain
[3]Materials Physics Center, CSIC-UPV/EHU and DIPC, San Sebastián 20018, Spain

Note: This paper is part of the Special Topic on Plasmonics: Enabling Functionalities with Novel Materials.
[a)]**Author to whom correspondence should be addressed:** Gaspar.armelles@csic.es

ABSTRACT

We present experimental and theoretical results of the molecular sensing performance of a novel platform based on magnetic modulation of surface-enhanced infrared absorption spectroscopy. For this, we study the effect that molecular infrared vibrations of a PMMA layer have on the optical and magneto-refractive response of spintronic antennas. Specifically, a periodic array of rods is fabricated from giant-magneto-resistance $Au/Ni_{81}Fe_{19}$ metallic multilayers, and the effect of depositing a layer of PMMA on top of the array is investigated from both experimental and theoretical points of view. We find that the relative changes induced by the infrared vibrations of PMMA on the magneto-refractive signal are larger than the relative changes induced on the optical transmission. This result indicates that the magneto-refractive response is more sensitive to the excitation of molecular vibrations than the optical response and fosters the development of a novel type of an infrared sensing technique based on spintronic antennas: Magneto-Refractive Surface-Enhanced Infrared Absorption (SEIRA) Spectroscopy.

I. INTRODUCTION

Plasmons have played a key role in the development of different types of optical sensing platforms. In the visible and near-infrared spectral range, Surface Plasmon Resonance (SPR) sensors or Localized Surface Plasmon Resonance (LSPR) sensors have exploited the sensitivity of plasmon resonances to changes of the refractive index in the regions near the metal surfaces.[1–4] Even though gold is commonly employed in these sensors, other types of metals, such as those of ferromagnetic nature, have also been used. The benefit of using ferromagnetic metals, in addition or substituting gold, is that they provide the system with Magneto Optical (MO) activity, which, in turn, is enhanced by the plasmon resonance.[5–9] Moreover, it has been shown that the MO properties of plasmonic structures can be more sensitive to changes of the refractive index than their optical counterpart, resulting in MO plasmonic sensors with increased sensitivity.[10–15] In the visible and near-infrared spectral range, the specificity of SPR or LSPR sensors to detect a particular molecule is determined by the functionalization of the surface. On the other hand, in the mid- and far-infrared, molecules show specific vibration bands that can be used to identify them, giving rise to a different type of sensing approach where plasmons play again a major role. In this approach, the vibration bands are used to directly detect and also unambiguously identify the molecules. To increase the signal of the vibrational band, the molecules are deposited on top of rough metallic surfaces, resulting in what is known as Surface-Enhanced Infrared Absorption (SEIRA)[16–18] spectroscopy. This signal can be further increased by nanostructuring the metallic surface or by using arrays of metallic antennas.[19,20] In all these surfaces, plasmons are responsible for the electromagnetic field enhancement at the position of the molecule, which results in the increase of the vibration signal. Very recently,

metasurfaces that support optical resonances in the mid- and far-infrared range have been fabricated out of Giant Magneto Resistance (GMR) metallic multilayers.[21–23] These spintronic–plasmonic metasurfaces have the peculiarity that their resonances can be modulated by applying a magnetic field. This is a consequence of the Magneto-Refractive Effect (MRE),[24,25] which accounts for the change in the optical constants of the GMR multilayer due to the modification of the electrical resistivity induced by the magnetic field [Fig. 1(a)]. Because of the direct role of conduction electrons in this phenomenon, the change in the optical constants covers from the mid-infrared to the THz regime, which may allow the development of magneto-active SEIRA surfaces, whose sensitivity could be further enhanced as compared to pure optical SEIRA surfaces.

In this work, we address the effect of magneto-refractive SEIRA by comparing the sensitivity of the optical and the magneto-refractive signals in GMR plasmonic SEIRA platforms to detect molecular vibrations. For this purpose, a model SEIRA surface consisting of an array of metallic rod antennas was fabricated out of a GMR Au/$Ni_{81}Fe_{19}$ multilayer [Figs. 1(b)–1(d)]. In the 5 μm−10 μm spectral range, the array has a resonance that can only be excited when light is polarized along the long axis of the rod [Fig. 1(c)]. It has a localized character (i.e., its position does not depend on the incident angle), and the electromagnetic field distribution corresponds to that of a dipolar resonance [Fig. 1(d)]. The array was then covered with a PMMA layer [Fig. 1(e)]. In this spectral range, PMMA has several vibration bands [Fig. 1(f)], which will be used to compare the sensitivity of the optical and magneto-refractive SEIRA signals to detect these vibrations.

II. RESULTS AND DISCUSSION

The Au/$Ni_{81}Fe_{19}$ multilayer (Ml) used to fabricate the rod antenna array was grown by magnetron sputtering from individual $Ni_{81}Fe_{19}$ and Au targets on a CaF_2(111) single crystalline substrate, which is highly transparent in this spectral range. Prior to the Ml growth, a 2 nm Ti buffer layer was deposited by electron beam evaporation. Details on the growth process can be found

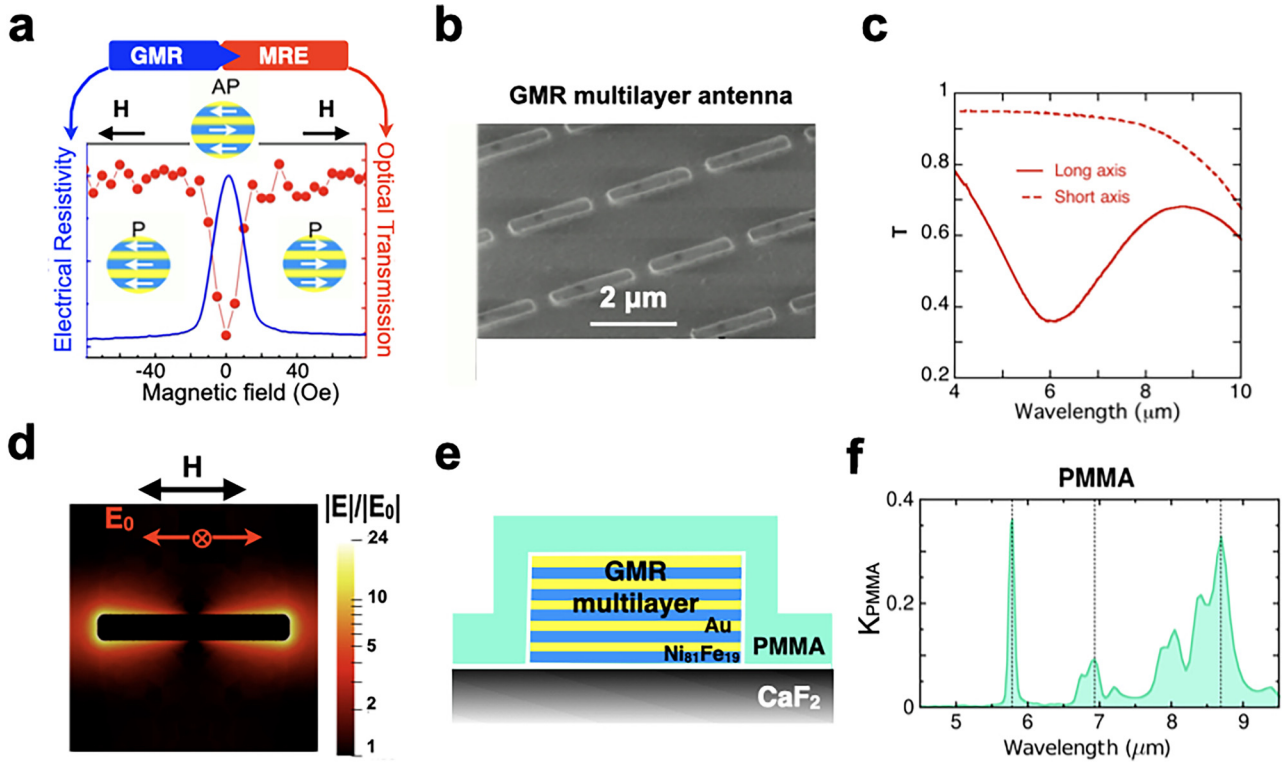

FIG. 1. (a) Magnetic-field dependence of the resistivity and infrared transmission in a GMR metallic multilayer. The multilayer is composed of alternating layers of non-ferromagnetic and ferromagnetic metals. When the magnetic moments of the adjacent ferromagnetic layers are antiparallel (AP), the resistivity is higher than when all the magnetic moments of the ferromagnetic layers are parallel (P). This change in the resistivity produces a change in the infrared optical properties: Magneto-Refractive Effect (MRE). (b) SEM image of the rod antenna array. (c) Transmission spectra for light polarized parallel (continuous line) and perpendicular (dashed line) to the long rod axis. (d) Color map of the electromagnetic field distribution at resonance, for incident light polarized along the long axis of the antenna, calculated in a plane parallel to the surface at the middle height of the rod and sketch of applied magnetic field (double black arrow on the top). (e) Sketch of the internal structure of the rods and morphology of the PMMA layer (represented as a conformal green layer) deposited on top of the rod used in the simulations. (f) Absorption coefficient of PMMA. The dashed vertical lines mark the position of the vibrational bands used in this work (see the text).

elsewhere.[26] The thicknesses of the individual Au and $Ni_{81}Fe_{19}$ layers are 2.3 nm and 2.9 nm, respectively, and the Au/$Ni_{81}Fe_{19}$ multilayer is characterized by a 4% GMR. The rod array was fabricated by electron beam lithography and Ar ion etching. The resulting structure is a square array of rods with a period of 2.6 μm. The rods in-plane dimensions are of 2 μm x 0.3 μm with a thickness of 60 nm [see Figs. 1(b) and 1(e)]. The PMMA layer was deposited by spin coating at 6000 rpm during 60 s using a solution of PMMA and anisole. After the deposition, the sample was heated to 180 °C for 5 min. The transmission spectrum of this system was measured via a Bruker 70 FTIR spectrometer.

In Fig. 2(a), we present the transmission spectra at normal incidence for light polarized along the long axis of the rods [as sketched in Fig. 1(d)] before (black line) and after (red line) the PMMA deposition. Both spectra show a dip due to the excitation of the rods' resonance around 6 μm. As expected, the position of the rod resonance covered with PMMA is located at a longer wavelength than that of the uncovered rods. Besides, in the spectrum of the rods covered with PMMA, additional features appear at the position of the PMMA bands. To highlight these features, in Fig. 2(b), we present the difference between this spectrum and the baseline (BL) one. This baseline spectrum, blue dotted line in Fig. 2(a), was obtained by smoothing the PMMA covered rod spectrum, i.e., by eliminating the effect of the PMMA vibrational bands while maintaining its effect on the change in permittivity of the surrounding medium. By comparing this difference with the imaginary part of the PMMA refractive index, K_{PMMA}, found in the literature (Ref. 27) and reported in Fig. 1(f), it becomes clear that there is a close relation between the complex features appearing in the difference spectrum and the absorption bands of the PMMA. For instance, a clear Fano-like structure is observed at 5.8 μm, where a sharp vibrational band of PMMA is located, and a more complex spectral shape is found in the regions around 6.9 μm and 8.4 μm, where PMMA shows several overlapping bands.

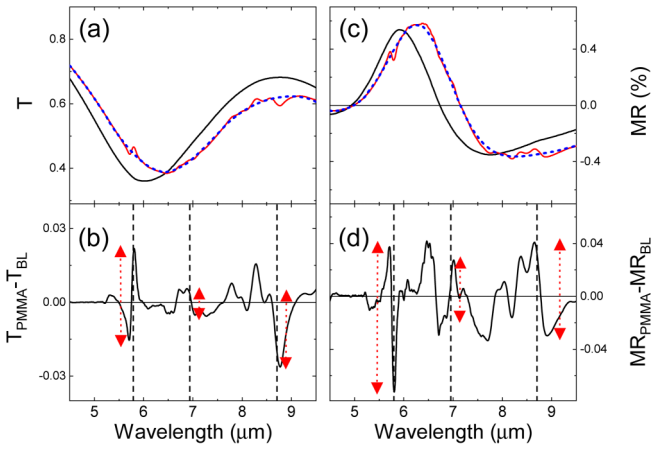

FIG. 2. (a) Experimental transmission spectra of the rod antenna array before (black line) and after (red line) PMMA deposition. The blue dotted line corresponds to the baseline optical spectrum with PMMA. (b) Difference between the transmission spectrum after the PMMA deposition and the baseline spectrum. The red arrows indicate the contrast of the vibrational features due to the bands at 5.8 μm, 6.9 μm, and 8.7 μm, respectively. The position of the concerned bands is marked by black dashed vertical lines. (c) Experimental magneto-refractive (MR) transmission spectra, $(T_P - T_{AP})/T_{AP}$ of the rod antenna array before (black line) and after (red line) PMMA deposition. The blue dotted line corresponds to the baseline MR spectrum. (d) Difference between the magneto-refractive transmission spectrum after the PMMA deposition and the baseline spectrum. The dashed red arrows indicate the contrast of the vibrational features due to the bands at 5.8 μm, 6.9 μm, and 8.7 μm, respectively. The position of the concerned bands is marked by dashed black vertical lines.

In Fig. 2(c), we present the corresponding magneto-refractive (MR) spectra (i.e., the relative difference of the transmission between the two resistivity states). The resistivity state of the multilayer was changed by applying an in-plane magnetic field along the long axis of the rods, as sketched in Fig. 1(d). At zero field, the magnetic moments of adjacent $Ni_{81}Fe_{19}$ layers are oriented along opposite directions (AP state), which correspond to the high resistivity state [Fig. 1(a)], whereas the low resistivity state is obtained by applying a magnetic field of 300 Oe, which allows a complete parallel alignment of the magnetic moments of all $Ni_{81}Fe_{19}$ layers (P state). The spectra were obtained at normal incidence, and the incident light was polarized along the long axis of the rods [see Fig. 1(d)]. The black and red lines correspond to the spectra before (black line) and after (red line) PMMA deposition, respectively. Both spectra have a S-like shape structure, being the structure after PMMA deposition shifted toward a longer wavelength with respect to the structure of the uncovered rods. Moreover, the spectrum of the rods covered with PMMA has additional features at the positions of the vibration bands of PMMA. These features are clearly seen in the difference spectrum shown in Fig. 2(d). The difference spectrum is defined as the difference between the MR of the system when coated with PMMA and the MR of the baseline spectra. By comparing this spectrum with the difference spectrum obtained previously in the optical signal, we observe that the features located in the 5.8 μm–6.7 μm spectral range have changed their sign; besides, the contrast of the features around 6.7 μm has increased. On the other hand, in the spectral region between 7.5 μm and 9 μm, there is a modification of the relative contrast of the different features, which gives rise to a change in the shape of the spectrum.

To quantify the relative change induced by the PMMA vibration bands on the optical and magneto-refractive signals over the whole spectral range of the rod resonance, we focused on the PMMA absorption bands located at 5.8 μm, 6.9 μm, and 8.7 μm, respectively (vertical black dashed lines of Fig. 2). For these bands, the intensity of the associated features is given by the length of the red dashed arrows depicted in Figs. 2(b) and 2(d), i.e., by the difference between the maximum and minimum value of the difference spectrum around the concerned wavelengths. The resulting relative change of the transmission difference is around 9%, 3%, and 5% for the three bands, respectively, whereas the relative change of the MR difference is around 27%, 30%, and 18% for the same three bands, respectively. These latter relative changes are between three and ten times larger than the former, leading to a magneto-refractive signal that is more sensitive to the presence of the vibration bands than the direct optical signal.

These experimental results are corroborated by theory, as demonstrated by numerical simulations of the effect of deposing a layer of PMMA on the optical and magneto-refractive signals of

the antenna array (see Fig. 3). The PMMA layer is assumed to cover the structure conformally, as shown in Fig. 1(e). For the optical characterization of the PMMA layer, we use the refractive index from Ref. 27 [Fig. 1(f)]. Under these conditions, a 55 nm thick PMMA layer reproduces the experimental red shift of the rod resonance (of about 460 nm), as seen by comparing Figs. 2(a) and 2(c) with Figs. 3(a) and 3(c), respectively. The baseline spectra were obtained by replacing the PMMA layer by a dielectric layer with the same thickness but with a refractive index of 1.46 and with no absorption. This dielectric layer simulates the effect of removing the vibration bands of PMMA but maintaining its background dielectric value as to obtain the same red shift of the rod resonance. Details on the rod structure model and on both the multilayer and substrate optical permittivities can be found elsewhere.[21] The calculated transmission of the system with (red solid line) and without (back solid line) the PMMA layer (as well as the baseline curve, blue dotted line) is displayed in Fig. 3(a) and reveals a plasmon dip around 6.5 μm and 6 μm, respectively. These dip positions agree with the experimental values [see Fig. 2(a)]. Moreover, the transmission of the system covered with PMMA shows features similar to those observed in the experiments. The calculation of the difference spectrum, shown in Fig. 3(b), highlights these features and clarifies their connections with the absorption bands of the PMMA [reported in Fig. 1(f)]. More importantly, the simulations reproduce the observed features, even though they are sharper and more intense than the experimental ones. In particular, the relative change in the difference transmissions for the bands located at 5.8 μm, 6.9 μm, and 8.7 μm is around 57%, 15%, and 18%, respectively. These values are higher than the experimental ones (namely, 9%, 3%, and 5%, respectively). The origin of this discrepancy may be due to the difference between the shape of the simulated and experimental rods and/or to the values of the refractive index of the PMMA layer. In the former case, the presence of sharp edges in the rod model results in near-field intensities much greater than the experimental ones, giving rise to an enhancement of the calculated vibration signals with respect to the experimental ones. Regarding the latter cause, the PMMA layer was deposited by spin coating using a diluted solution of PMMA; therefore, the strength of the vibration bands in the deposited layer could be smaller than that of the PMMA film from where the refractive index was extracted (Ref. 27), resulting in an overestimation of the intensity of the vibrations. A similar effect has been found in other SEIRA works where the PMMA was also deposited using a solution of PMMA in anisole.[28]

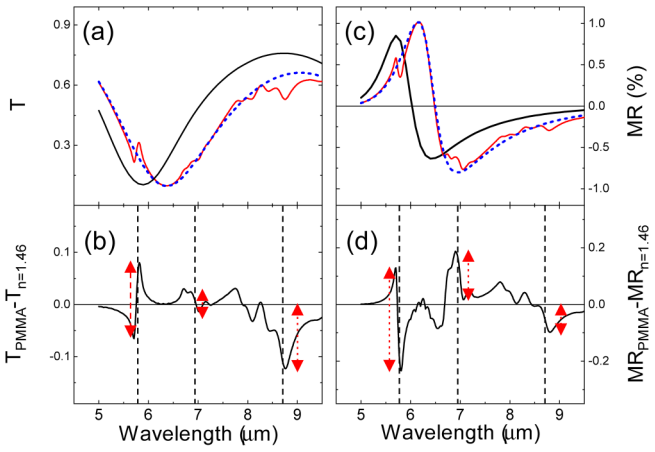

FIG. 3. (a) Simulated transmission spectra of the rod antenna array without PMMA (black line) and with a 55 nm thick PMMA layer covering the rod array (red line). The blue dotted line corresponds to the spectrum obtained by replacing the PMMA by a dielectric material with a refractive index of 1.46. (b) Difference between the PMMA transmission spectrum and the n = 1.46 transmission spectrum. The red dashed arrows indicate the contrast of the vibrational features due to the bands at 5.8 μm, 6.9 μm, and 8.7 μm, respectively. The position of the concerned bands is marked by black dashed vertical lines. (c) Simulated magneto-refractive transmission spectra, $(T_P - T_{AP})/T_{AP}$, of the rod antenna array without (black line) and with (red line) PMMA. The blue dotted line corresponds to the spectrum obtained replacing the PMMA by a n = 1.46 dielectric material. (d) Difference between the magneto-refractive transmission spectrum with PMMA and with a n = 1.46 dielectric layer. The red dashed arrows indicate the contrast of the vibrational features due to the bands at 5.8 μm, 6.9 μm, and 8.7 μm, respectively. The position of the concerned bands is marked by black dashed vertical lines.

In Fig. 3(c), we plot the results for the MR spectrum of the considered systems. The curve shift and the presence of specific features for the MR response of the system covered with PMMA agree with the experimental results. However, the calculation of the MR difference spectrum [Fig. 3(d)] also reveals higher feature intensities as compared to the experimental ones [Fig. 2(d)]. The same reasons as those stated above for the difference found between simulated and measured transmissions stand in this case [Figs. 3(b) and 2(b), respectively]. The relative change of the magneto-refractive difference signal, found to be 64%, 26%, and 50% for the three vibration bands, respectively, is also a bit larger than the experimental counterpart. Nevertheless, and more importantly, these values are between 1.1 and 2.7 times higher than the relative changes of the transmission difference spectrum, thus corroborating that the magneto-refractive signal (MR) is more sensitive to the presence of the vibration bands than the optical one (T).

III. CONCLUSIONS

The effect that a layer of PMMA deposited on top of a spintronic–plasmonic antenna array has on its infrared transmission and its magneto-refractive signal has been experimentally and theoretically addressed. The deposition of a PMMA layer on this array leads to a redshift of the plasmon resonance and to a featured line shape for both the optical and the magneto-refractive signals. The found features are due to the excitation of vibrational bands of the PMMA. Significantly, we showed that the relative changes induced by the vibrational bands of the PMMA in the magneto-refractive signal are higher than the relative changes induced in the infrared transmission. In these magneto-active SEIRA metasurfaces, the vibrations can thus be detected using the magneto-refractive signal (magneto-refractive SEIRA) instead of the pure optical one. These results indicate that GMR plasmonic metasurfaces could be used to enhance the sensitivity of SEIRA platforms and pave the path to a

new type of transducers, where the connection between spintronics and photonics results in more sensitive sensors.

ACKNOWLEDGMENTS

We acknowledge financial support from MINECO through projects AMES (No. MAT 2014-58860-P), Quantum Spin Plasmonics (No. FIS2015-72035-EXP), and MIRRAS (No. MAT2017-84009-R) and Comunidad de Madrid (CM) through project SINOXPHOS-CM (No. S2018/BAA-4403). We acknowledge the service from the MiNa Laboratory at IMN and funding from MINECO under Project No. CSIC13-4E-1794 and from CM under Project No. S2013/ICE-2822 (Space-Tec), both with support from EU (FEDER, FSE). L.B., N.Z., and J.A. acknowledge support from the Department of Education, Research and Universities of the Basque Government through Project Ref. No. IT-1164-19, the Department of Industry of the Basque Government through Project No. KK-2018/00001, and the Spanish MICIN through Project Ref. No. PID2019-107432GB-I00.

DATA AVAILABILITY

The data that support the findings of this study are available from the corresponding author upon reasonable request.

REFERENCES

[1]J. Homola, Chem. Rev. **108**, 462 (2008).
[2]A. G. Brolo, Nat. Photonics **6**, 709 (2012).
[3]J. N. Anker, W. P. Hall, O. Lyandres, N. C. Shah, J. Zhao, and P. Van Duyne, Nat. Mater. **7**, 442 (2008).
[4]B. Sepúlveda, P. C. Angelomé, L. M. Lechuga, and L. M. Liz-Marzán, Nano Today **4**, 244 (2009).
[5]G. Armelles, A. Cebollada, A. García-Martín, and M. U. González, Adv. Opt. Mater. **1**, 10 (2013).
[6]D. Bossini, V. I. Belotelov, A. K. Zvezdin, A. N. Kalish, and A. V. Kimel, ACS Photonics **3**, 1385 (2016).
[7]I. Maksymov, Nanomaterials **5**, 577 (2015).
[8]D. Floess and H. Giessen, Rep. Prog. Phys. **81**, 116401 (2018).
[9]N. Maccaferri, I. Zubritskaya, I. Razdolski, I. A. Chioar, V. Belotelov, V. Kapaklis, P. M. Oppeneer, and A. Dmitriev, J. Appl. Phys. **127**, 080903 (2020).
[10]B. Sepúlveda, A. Calle, L. M. Lechuga, and G. Armelles, Opt. Lett. **31**, 1085 (2006).
[11]D. Regatos, D. Fariña, A. Calle, A. Cebollada, B. Sepúlveda, G. Armelles, and L. M. Lechuga, J. Appl. Phys. **108**, 054502 (2010).
[12]M. G. Manera, E. Ferreiro-Vila, J. M. Garcia-Martin, A. Garcia-Martin, and R. Rella, Biosens. Bioelectron. **58**, 114 (2014).
[13]N. Maccaferri, K. E. Gregorczyk, T. V. A. G. de Oliveira, M. Kataja, S. van Dijken, Z. Pirzadeh, A. Dmitriev, J. Åkerman, M. Knez, and P. Vavassori, Nat. Commun. **6**, 6150 (2015).
[14]B. Caballero, A. García-Martín, and C. Cuevas, ACS Photonics **3**, 203 (2016).
[15]D. O. Ignatyeva, G. A. Knyazev, P. O. Kapralov, G. Dietler, S. K. Sekatskii, and V. I. Belotelov, Sci. Rep. **6**, 2877 (2015).
[16]A. Hartstein, J. R. Kirtley, and J. C. Tsang, Phys. Rev. Lett. **45**, 201 (1980).
[17]M. Osawa, "Surface-enhanced infrared absorption," in *Near-Field Optics and Surface Plasmon Polaritons*, edited by S. Kawata (Springer, Berlin, 2001).
[18]R. F. Aroca, D. J. Ross, and C. Domingo, Appl. Spectrosc. **58**, 324A (2004).
[19]F. Neubrech, A. Pucci, T. W. Cornelius, S. Karim, A. García-Etxarri, and J. Aizpurua, Phys. Rev. Lett. **101**, 157403 (2008).
[20]F. Neubrech, C. Huck, K. Weber, A. Pucci, and H. Giessen, Chem. Rev. **117**, 5110 (2017).
[21]G. Armelles, L. Bergamini, N. Zabala, F. García, M. L. Dotor, L. Torné, R. Alvaro, A. Griol, A. Martínez, J. Aizpurua, and A. Cebollada, ACS Photonics **5**, 3956 (2018).
[22]G. Armelles, L. Bergamini, N. Zabala, M. U. Gonzalez, F. Garcia, R. Alvaro, J. Aizpurua, and A. Cebollada, Nanophotonics **8**, 1847 (2019).
[23]G. Armelles, L. Bergamini, A. Cebollada, M. U. Gonzalez, R. Alvaro, L. Torne, N. Zabala, and J. Aizpurua, Opt. Express **28**, 32584 (2020).
[24]J. C. Jacquet and T. Valet, Mater. Res. Soc. Symp. Proc. **384**, 477–490 (1995).
[25]G. Armelles and A. Cebollada, Nanophotonics **9**, 2709 (2019).
[26]G. Armelles, A. Cebollada, and F. García, Opt. Mater. Express **9**, 923 (2019).
[27]X. Zhang, J. Qiu, J. Zhao, X. Li, and L. Liu, J. Quant. Spectrosc. Radiat. Transf. **252**, 107063 (2020).
[28]F. Cheng, X. Yang, and J. Gao, Sci. Rep. **5**, 14327 (2015).